Ann. Geophysicae 10, 309–322 (1992)

Annales Geophysicae

Evidence for strange attractor structures in space plasmas

G. P. Pavlos [1], G. A. Kyriakou [1], A. G. Rigas [1], P. I. Liatsis [1], P. C. Trochoutsos [1], and A. A. Tsonis [2]

[1] Department of Electrical Engineering, Demokritos University of Thrace, 67100 Xanthi, Greece
[2] Department of Geosciences, University of Wisconsin, Milwaukee, WI 53201, USA

Received July 2, 1991; revised December 23, 1991; accepted January 8, 1992

Abstract. In this study we apply modern methods for the search of strange attractor structures with low dimension to space plasmas. Together with an estimation of the correlation dimension, we include in our methods an estimation of the largest Lyapunov exponent and the development of reliable criteria for the exclusion of pseudochaotic dynamics caused by colored noises. The use of these methods in the analysis of magnetospheric and solar wind data gives strong evidence for low-dimensional chaotic dynamics. In particular, our findings indicate a magnetospheric strange attractor with a fractal dimension of about 3.5 and a solar wind strange attractor with a fractal dimension of about 4.5.

Introduction

The recent development of chaotic dynamics of non-linear and dissipative systems (Eckman and Ruelle, 1985) provides us with a new tool which permits the distinction between deterministics and random noise. Thus, in many physical processes, the infinitely quasiperiodic spectrum of excited models must be replaced by new concepts such as non-negative Lyapunov exponents, information dimension, correlation dimension, etc. The unifying concept in all these methods is the strange attractor structure. In chaotic dynamics, the evolution of a physical system in phase space, once transients die out, settles on a submanifold which is a fractal set (the strange attractor) of zero volume (in some appropriate phase space). The motion of the dissipative system in this limited region of phase space may be unstable because of exponential divergence of initially nearby orbits. This exponential separation can be quantified by the Lyapunov exponents. Because of these characteristics, even though a chaotic system can be described by a low-dimensional deterministic system, its long-term predictability is not guaranteed.

Offprint requests to: G. P. Pavlos

One of the most important goals in space physics is to understand how basic elements work in the solar wind-magnetosphere-ionosphere interaction. The main manifestations of this interaction are magnetospheric substorms, as a collective and global response of the magnetosphere and ionosphere to a set of conditions in the solar wind. Characteristically, we mention typical events during a substorm expansive phase such as a sudden brightening of equatorward aurora, the intensification of field-aligned currents and of the westward-eastward auroral electrojet currents, plasma sheet thinning, an eartwarth injection of energetic electrons and ions, energetic particle bursts in the magnetotail, high-speed bursts of earthward-tailward plasma flow (500–1000 m/s) in the central plasma sheet, the intensification of magnetohydrodynamic (MHD) waves in different regions of the magnetosphere, and plasma turbulence (McPherron, 1979; Rostoker, 1987; Pavlos and Sarris, 1989; Pavlos *et al.*, 1989).

The motion of the magnetospheric state on a strange attractor was previously considered as an explanatory paradigm for all magnetospheric dynamics (Pavlos, 1988). Baker *et al.* (1990) showed that the motion of the magnetospheric state throughout a three-dimensional chaotic attractor, in analogy to Shaw's faucet model (Shaw, 1984), could successfully model and explain many of the observed substorm characteristics. Vassiliadis *et al.* (1990) and Shan *et al.* (1991) used AE index measurements to estimate magnetospheric chaos. However, their results are contradictory for the correlation dimension of the AE index.

The solar wind is the continuous expansion of solar corona plasma into interplanetary space. It can be described as a magnetization fluid with complex fluid and magnetic structures, such as high speed streams, evolving shock waves, the heliomagnetic neutral sheet, magnetic loops or clouds, magnetic field fluctuations and irregularities (Hundhausen, 1972). It is obvious that the solar wind and the magnetospheric-inospheric medium constitute highly turbulent and noisy physical systems, with notable backgrounds of broadband spectra. Burlaga (1991) studied large scale magnetic field fluctuations and found a

multifractal structure of the interplanetary magnetic field. However, this result was explained mainly as "colored noise".

Here, we extend previous studies by using a more complete form of chaotic analysis. In particular, we expand the correlation dimension analysis used in the works of Vassiliadis *et al.* (1990) and Shan *et al.* (1991), by computing not only the correlation dimension, but also the largest Lyapunov exponents and the three-dimensional phase portraits for different kinds of magnetospheric data. Moreover we develop some new criteria to eliminate the possibility of pseudochaotic dynamics, which could be caused by noisy data exhibiting a power spectrum of the form f^{-a}. All these extended methods of chaotic analysis are also applied in the case of solar wind data. Thus, by using chaotic analysis in its general form, we present strong evidence for the existence of magnetospheric and solar wind strange attractor structures with fractal dimensions of about 3.5 and about 4.5 respectively.

Data analysis

Analysis in the time and the frequency domain

The theory of nonlinear dynamical systems provides a new way of analyzing a nonperiodic time series in order to distinguish between "deterministic" and "random" physical signals. The power spectrum $S(\omega)$ of a scalar signal $x(t)$ can show whether a system is periodic or quasiperiodic (with basic frequencies $\omega_1, \ldots, \omega_c$) but it cannot provide any information for a broadband spectrum. Only in the extreme case of a random signal which is white noise the power spectrum density is independent of the frequency. A chaotic deterministic signal $x(t)$ exhibits a power spectrum with a continuous part indicating that the time evolution of the quantity $x(t)$ is disordered and erratic (Farmer, 1981; Eckman, 1981). Also the spectrum analysis does not explain whether the broadband component of a spectrum is caused by an quasiperiodic attractor (i.e. a torus T^k of sufficiently high dimension k), or by a low dimension chaotic attractor.

The same thing happens with the autocorrelation coefficient

$$\varrho(\tau) = \frac{C(\tau)}{C(0)},$$

where

$$C(\tau) = \langle x(t+\tau)\, x(t)\rangle - \langle x(t+\tau)\rangle \langle x(\tau)\rangle,$$

which, according to the Wiener-Khintchine theorem, is the Fourier transform of the power spectrum. The autocorrelation coefficient remains nonzero (as the lag time τ tends to infinity) for a periodic or quasiperiodic signal, but tends to zero as the lag time increases for a deterministic random or stochastic random nonperiodic signal whose power spectrum includes a continuous part.

Strange attractor analysis

The embedding theorem of Takens (1981), the fractal dimension of the strange attractor and the positive Lyapunov exponents are the basic tools for the experimental estimation of the chaotic dynamics of an observed physical system. According to Takens, if the dynamics of a complex system (in our case, the magnetosphere or solar wind) can be reduced to a k-dimensional flow described by the differential equations

$$\mathrm{d}\boldsymbol{x}(t)/\mathrm{d}t = \boldsymbol{F}(\boldsymbol{x}(t), \lambda_\mu),$$

where $\boldsymbol{x}(t) \equiv \{x_1(t), x_2(t), \ldots, x_k(t)\}$ is the vector of the observable dynamic variables of the system and λ_μ are the control parameters, then this flow and some of its properties can be experimentally reconstructed from the observed time series of a single observable dynamic component $x(t)$. From a discrete time series, $x_n = x(t_n)$, $n = 1, 2, \ldots, N$, measured experimentally, the vector construction

$$\xi(t_n) = \{x(t_n), x(t_n + \tau), \ldots, x[t_n + (2D+1)\tau]\}$$

gives a smooth embedding of the flow in a $(2D+1)$-dimensional phase space. The reconstructed trajectory $\xi(t_i)$ provides a topological approximation to the D-dimensional attractor in the real phase space (assuming that an attractor exists).

The reconstruction time τ is a suitable delay parameter, often taken to be equal to the decorrelation time of the signal x_n. The experimental estimation of a strange attractor and its fractal dimension can be obtained using the correlation integral $C(r; m)$ proposed by Grassberger and Procaccia (1981). This quantity is defined for a m-dimension embedding space of the experimentally-reconstructed trajectory

$$\xi(t_i) = \{x(t_i), x(t_i + \tau), \ldots, x[t_i + (m-1)\tau]\}$$

by the equation

$$C(r; m) = \lim_{N \to \infty} \frac{1}{N^2} \quad \{\text{the number of pairs of points } \xi(t_i) \text{ and } \xi(t_j) \text{ such that } \|\xi_i - \xi_j\| < r\}.$$

The correlation dimension D of the attracting submanifold in the reconstruction phase space is given by the equation

$$D = \lim_{r \to 0, m \to \infty} \frac{d(\ln C(r; m))}{d(\ln r)},$$

where m denotes the embedding dimension. This quantity weights a volume element in the attractor according to how often a trajectory is found in it (Schuster, 1989). In data analysis, where random noise is present, there is a statistically significant scaling region $(r_0 - r_1)$ extending from r_0 (minimum value) to r_1 (maximum value), where the slope $d(\ln C(r; m))/d(\ln r)$ remains constant and a plateau is observed. This gives a real measure of the correlation dimension if the embedding dimension m is suitably large. For r smaller than r_0, we have a large scatter of points due to poor statistics, while for r larger than r_1 there is a deviation from a constant slope due to nonlin-

ear effects. Thus, for the case of a chaotic signal (exhibiting a strange attractor), there is a saturation of the slope $d(\ln C(r; m))/d(\ln r)$ according to the power law $C(r; m) \propto r^D$, which is true for the scaling region with no change of the slope D and for embedding dimensions m higher than some embedding dimension m_0.

If the observed time series $x(t_n)$ is purely random with no systematic informational effect, there is no such saturation of the correlation dimension, and $C(r; m) \propto r^m$ as m increases. The existence of a scaling region with a meaningful plateau depends greatly on the amount of data (time series length). Smith (1988) had argued that the minimum number of independent data points required ($N_{\min}$) is of the order of $N = 40^D$. Recently it has been estimated that, in cases where an attractor of dimension S exists, a $N_{\min}$ is given by $N \cong 10^{(2+0.4D)}$ (Nerenberg and Essex, 1990). Another tool in searching for evidence about the existence of strange attractors is the Lyapunov exponents, which are defined as the long-term evolution of the axes of an infinitesimal sphere of states in phase space. For chaotic systems, neighbouring orbits in phase space diverge exponentially, a property known as sensitivity to initial conditions (Parker and Chua, 1987). According to this, any dynamic system containing at least one positive Lypunov exponent is defined to be chaotic. The magnitude of the positive exponent gives the scale on which the dynamics of the system become unpredictable. Here we followed the work of Wolf *et al.* (1985) to obtain an estimation of the largest Lyapunov exponent, $L_{\max}$, which is defined by the relation

$$L_{\max} \cong (1/t_M - t_0) \sum_{i=1}^{M} \log_2 (L'(t_i)/L(t_{i-1}))$$

$L(t_i)$ denotes the distance which separates two nearby trajectories in the reconstructed phase space following M steps on the fiducial trajectory. The previously described chaotic analysis of a real time series in the estimation of the correlation dimension and the largest Lyapunov exponent runs into some difficulties which partially weaken the efficiency of our analysis for the experimental study of chaos. Osborne and Provenzale (1989) studied colored noise time series described by

$$X(t_i) = \sum_{i=1}^{M/2} C_k \cos(\omega_k t_i + \varphi_k), \quad i = 1, \ldots, M,$$

where the phases φ_k are randomly distributed on the interval $[0, 2\pi]$ and C_k are constants related to the power spectrum $P(\omega_k)$ by

$$C_k = \left[P(\omega_k) \frac{2\pi}{M} \frac{1}{\Delta} \right]^{1/2}.$$

These random time series have power spectra $P(\omega)$ of the form ω^{-a} and show low-dimensional chaos, with the correlation dimension D related to α through the relation $D = 2/(a-1)$. An obvious step in our study of space plasma time series is to compare the chaotic characteristics of real time series with the pseudo-chaotic characteristics of colored noise time series. This has led us to the development of some criteria for the distinction between noisy and chaotic behaviour of real data.

In the following we apply the above methodologies to four kinds of data:

(i) The AE index with one-minute time resolution.
(ii) In situ magnetic field measurements in the magnetotail with 1-s time resolution made by the Goddard Space Flight Center (GSFC) fluxgate magnetometer on board the IMP-8 spacecraft.
(iii) Hourly averaged interplanetary plasma proton temperature (T) and magnetic field (B) measured in situ at 1 AU.

Magnetospheric low-dimensional chaotic dynamics

Chaotic analysis of the AE index and the plasma sheet magnetic field time series

Figure 1a shows the time series for the AE index data measured during January 1985, the corresponding autocorrelation coefficient and the power spectrum. During roughly 333 hours (20 000 min) of AE index measurements, we observe a variety of strong and weak substorms. The duration of a substorm event is about 30–60 min, while, for the entire period, more than 200 discrete substorm events are included. The autocorrelation coefficient shown in Fig. 1b (solid line) drops to lower than $1/e$ of its maximum during the first 100 min of lag time, while its first zero is observed at 1900 min of lag time. The curve shown by stars in the same figure corresponds to the autocorrelation coefficient of a colored noise with the same correlation dimension (3.5) as the AE data. The decrease in the autocorrelation coefficient of the colored noise for small lag times happens slowly, in contrast to the AE autocorrelation coefficient which decreases abruptly. In particular, the AE autocorrelation coefficient decreases to $1/e$ of its initial value after about 100 min, while the same decrease for the colored noise data is observed after about 500 units of lag time (min). Moreover, the decorrelation times for the AE and colored noise time series are different, about 2000 and about 1400 respectively. Figure 1c shows the power spectrum of the AE time series. All the spectra shown were smoothed by using a Parzen window (Brillinger, 1981). The spectral density reveals a power law $P(f) \propto f^{-a}$, with a broadband form for frequencies $f > 10^{-4.5}$ Hz. The estimated value of the exponent a is 1.9 ± 0.05 (see Fig. 1c). Figure 2a shows the logarithm of the correlation integral $C(r; m)$ against the logarithm of r for a reconstructed phase space with embedding dimension $m = 4-7$. The best scaling $C(r; m) \propto r^D$, for the AE time series was found when a delay time of 150 min was used in the reconstruction of the state vectors $X(t) = \{X(t), X(t+\tau), \ldots, X[t+(m-1)\tau]\}$. Figure 2b shows the corresponding slopes $\Delta \ln C(r; m)/\Delta \ln(r)$ against $\ln(r)$. It can be observed that, for $m \geq 4$, the slope over the scaling region (plateau region) $\ln(r) < 4$ remains constant at a D of about 3–3.5. For embedding dimensions $m < 4$, the slope increases as m increases. The saturation value of the slope $D = 3-3.5$ was found to be invariant under a change in the number of points, N, of the used time series. Testing with different values of N (5000–

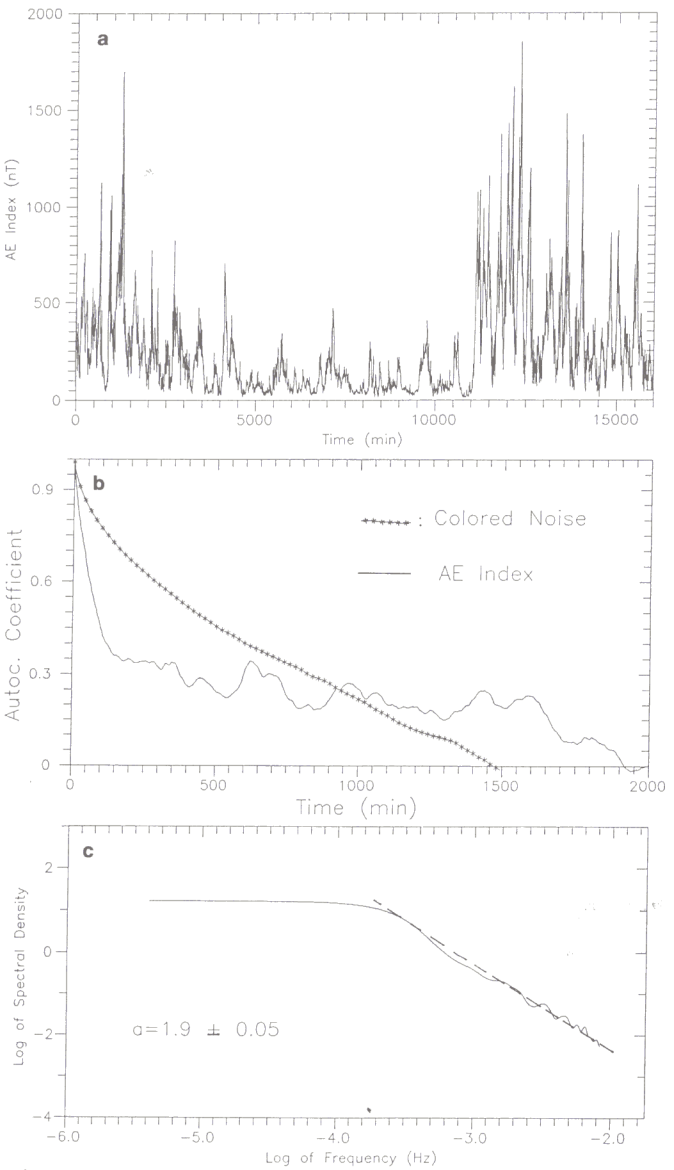

Fig. 1. **a** AE index time series with 1 min time resolution. **b** The autocorrelation coefficient of the AE time series and the autocorrelation coefficient of a colored noise with fractal dimension $D \simeq 3.5$, **c** the power spectrum of the AE time series

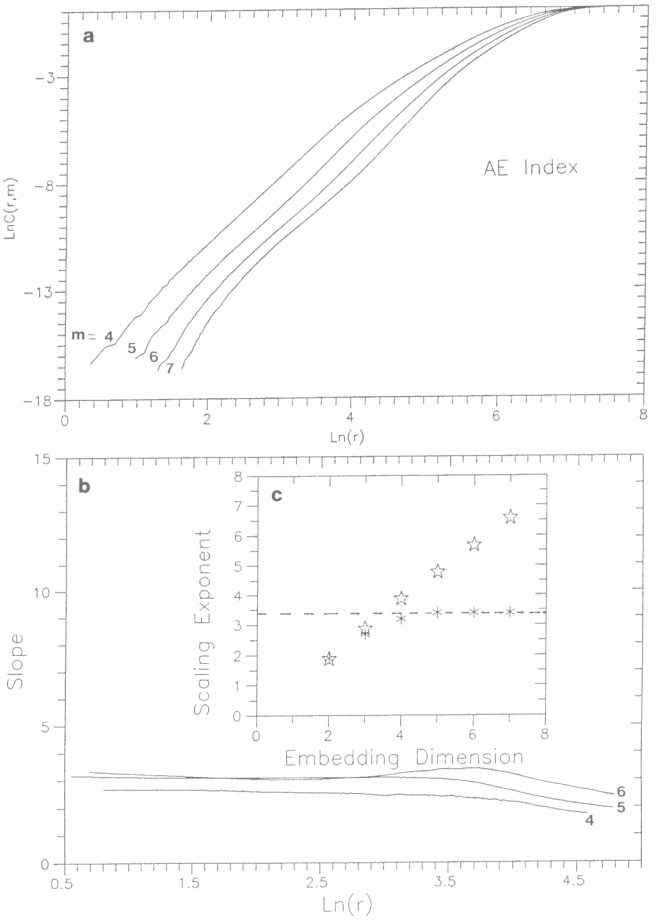

Fig. 2. **a** The correlation integral $C(r;m)$ of the AE time series for embedding dimensions $m = 2, 3, 4, 5$, **b** slopes $\Delta \ln C(r;m)/\Delta \ln r$ for $m = 3, 4, 5$, **c** the scaling exponent as a function of the embedding dimension m for the AE data (stars) and the random data (open stars)

30 000) justified the assertion of $N_{\min}$ being $10^{2+0.40D}$. Figure 2c summarizes the results of the correlation dimension analysis. It shows the scaling exponent of the correlation integral as a function of m for the AE data (stars) and a random sample (open stars) of the same size as the AE sequence. The random sample was constructed by randomizing the original AE sequence. This was done by using a subroutine which generates random numbers. It is clear that, for the random sample, there is no saturation of the scaling exponent, while with the AE index data there is a saturation at a D of about 3.4.

During days 280–281 in 1974, the spacecraft IMP-8 was traversing the earth's magnetotail at a distance of about 40 Re, remaining in the plasma sheet for some time. This region is known to be strongly turbulent, especially during substorm events (Pavlos and Sarris, 1989; Pavlos et al., 1989). In situ measurements of the plasma sheet magnetic field B revealed a strongly erratic character, as we show in Fig. 3a. In the plasma sheet, the magnetic field was less than 20 nT, but frequently the spacecraft moved far from the plasma sheet to the near lobes where $\boldsymbol{B}$ exceeded 20 nT. The length of this magnetic field time series N is 9000 points. Figure 3b shows that the first zero value of the autocorrelation coefficient is at 500 s, while a $1/e$ decrease is observed after 10 s. These characteristic values are remarkably different for a colored noise (the curve shown by squares) with the same fractal dimension as the $\boldsymbol{B}$ data. As for the power spectrum shown in Fig. 3c, we can distinguish two regions of frequencies with different power law exponents. For frequencies under $10^{-1.5}$ Hz, a is about 1.25 ± 0.8 and for frequencies above $10^{-1.5}$ Hz, a is 0.5 ± 0.3. Figure 4a–c presents the correlation dimension analysis for the magnetotail magnetic field. It is clear that there is a saturation value for the slope $D = \Delta \ln C(r;m)/\Delta \ln(r) \simeq 3.5$ at the scaling region $\Delta \ln(r) \simeq (-2) - (1.5)$. The best delay time, τ, used for the reconstruction of state vectors $\{B(t), B(t+\tau), \ldots, B[t+(m-1)\tau]\}$ is 10 s. For random data (open squares) no saturation is observed.

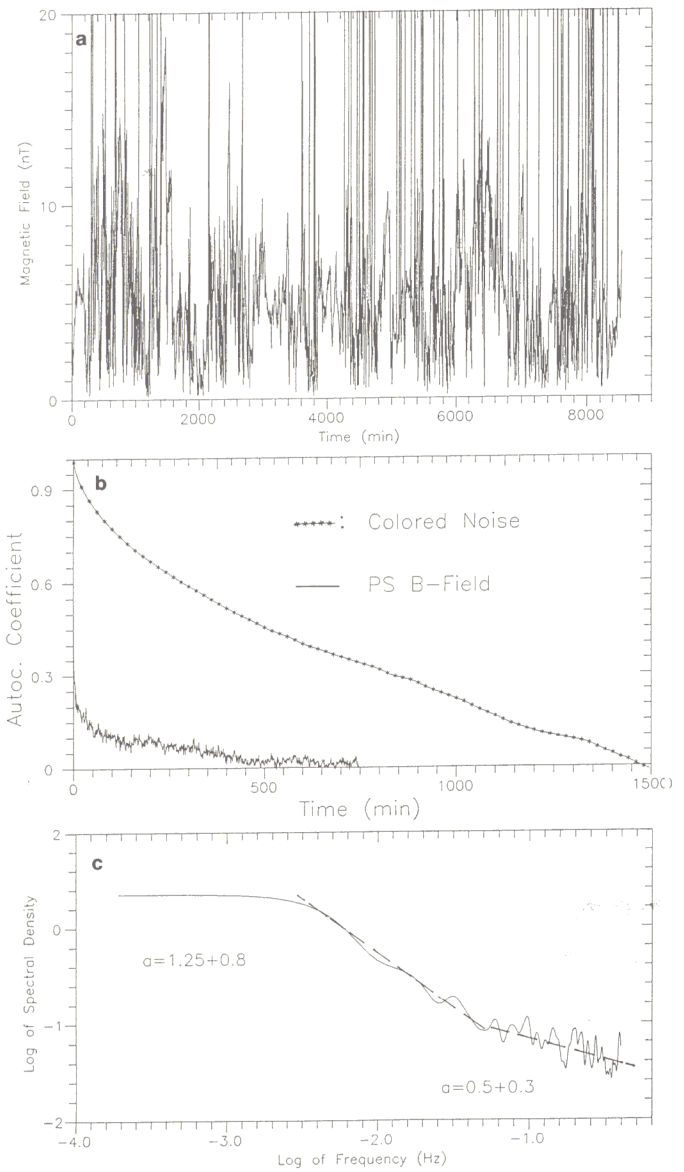

Fig. 3a–c. Same plots as in Fig. 1 for the magnetotail plasma sheet magnetic field (PS ***B***-field) time series

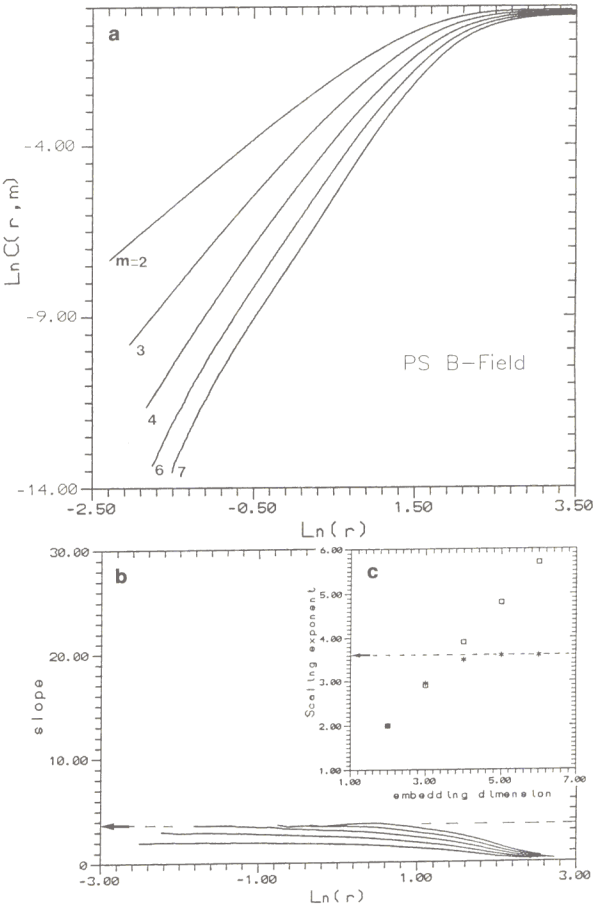

Fig. 4a–c. Same plots as in Fig. 2 for the plasma sheet ***B***-field time series obtained for embedding dimensions $m = 2, 3, 4, 5, 6$

Figure 5 shows an estimate of the largest Lyapunov exponent, L_{max}, for the AE time series (Fig. 5a) and for the magnetotail field measurements (Fig. 5b). For the AE data, L_{max} stabilizes at 0.23 bit/min, when the evolution time step in Wolf's algorithm is 3, and at 0.1 bit/min when the evolution step is 8. In the magnetic field case, L_{max} stabilizes at 0.4 bit/sec and 0.1 bit/min respectively. Figure 5c showed the estimate of L_{max} for a colored noise time series having the same correlation dimension with the AE and ***B*** field data. It is obvious that the L_{max} of the colored noise data is approximately 10 times lower than the L_{max} of the real data. Also, for the colored noise time series there is a very small difference between the Lyapunov exponents obtained for evolution time steps of 3 and 8. The variations ΔL_{max} are approximately: a) 0.014 for the colored noise; b) 0.14 for the AE time series; and c) 0.3 for the ***B***-field time series.

Discussion

The low fractal dimension of 3.5 calculated for the AE and the magnetotail magnetic field data, as well as the positive values for the largest Lyapunov exponent in both time series, strongly support the existence of a strange attractor structure in magnetospheric dynamics. This supposition can be further strengthened by noting the following characteristics of chaotic dynamics discussed previously:

a) The autocorrelation coefficient of the real time series (AE and magnetotail ***B*** field data) quickly drops to $1/e$ of its maximum, in contrast to a colored noise time series with the same fractal dimension as the real ones, which shows a very slow decrease in the autocorrelation coefficient.

b) The Lyapunov exponents, L_{max}, of the AE and ***B*** field data stabilize at positive values which are one order of magnitude higher than the corresponding L_{max} of the colored noise data. Also, the variation ΔL_{max}, which corresponds to values of L_{max} estimated with different evolution steps (3 and 8) for the AE and ***B*** field time series, it approximately 10–30 times higher than the corresponding ΔL_{max} for the colored noise time series.

c) The power spectra of the AE and ***B*** field data follow a power law $P(f) \propto f^{-a}$, with α being roughly 1.9 ± 0.05

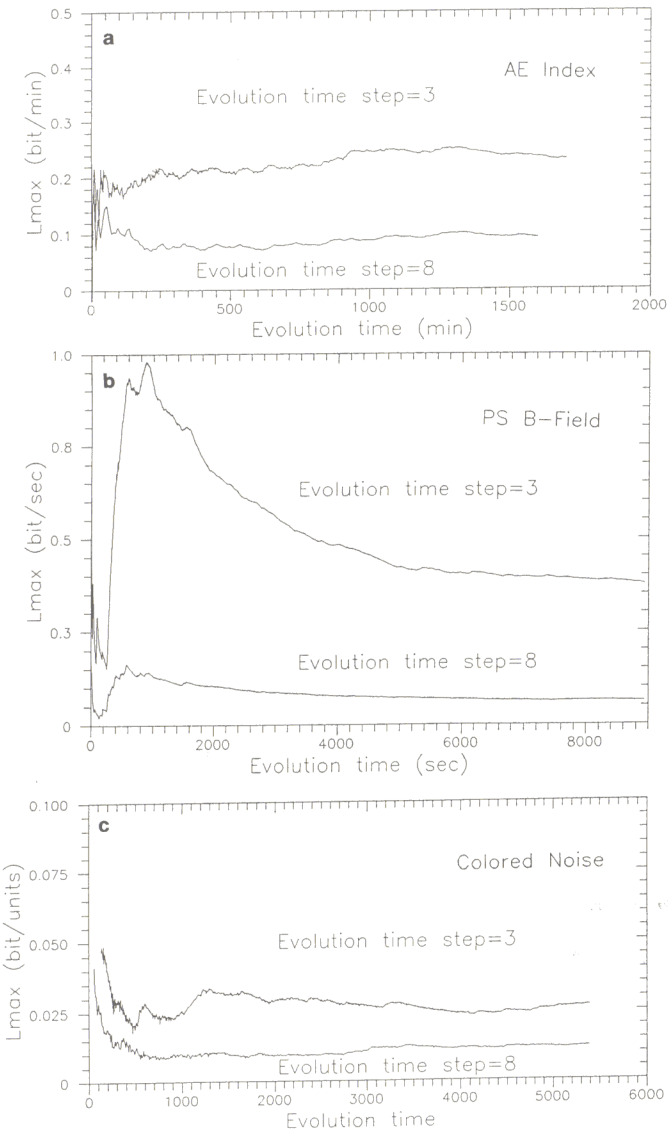

Fig. 5a–c. The largest Lyapunov exponent L_{max} for two different evolution steps as a function of the evolution time for **a** the AE time series, **b** the PS ***B***-field time series and **c** a colored noise with similar fractal dimension to the AE and ***B***-field data (3.5)

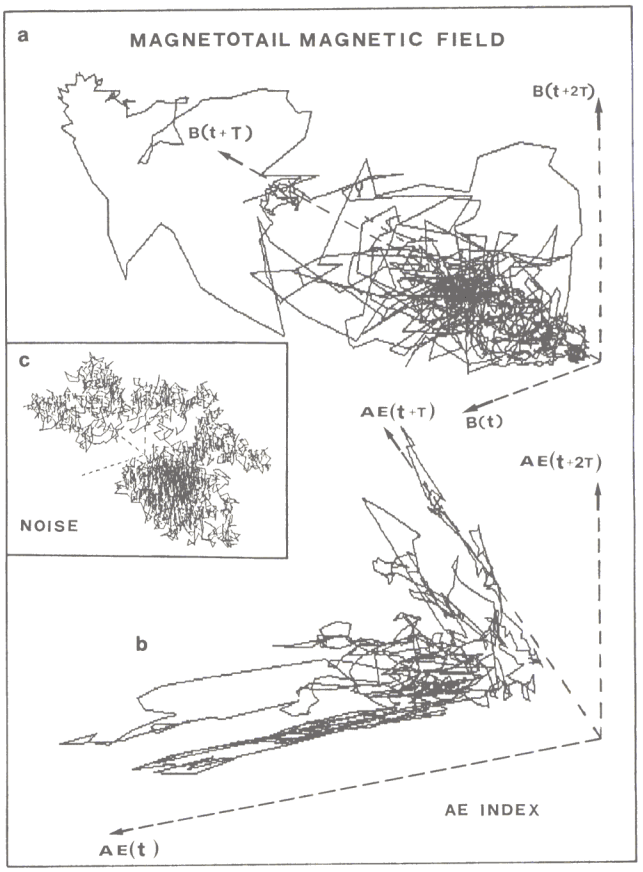

Fig. 6a–c. Three-dimensional phase portaits for: **a** the magnetotaill magnetic field time series, **b** the AE index time series and **c** a colored noise with similar fractal dimension to that of the magnetospheric data

for the AE data and roughly 1.25 ± 0.1 for the ***B*** field data. If we suppose that the power law profile of these spectra is mainly caused by colored noises of the form studied by Osborne and Provenzale (1989), then the corresponding correlation dimensions should be about 2.2 ± 0.2 and 8 ± 2 respectively. However, these values are quite different from the correlation dimensions of 3.4 and 3.6 found above.

d) The correlation dimensions obtained by using AE data taken on earth and ***B*** field data taken in situ, in the plasma sheet 40 Re from the earth, are almost identical, being 3.4 and 3.6 respectively. This is an impressive similarity.

The characteristics (a) and (b) are in accordance with a sensitivity to initial conditions characteristic of a system evolving on a strange attractor structure. According to this principle, the displacement $L(t_i)$ of two nearby orbits quickly increases for small values of the evolution time step $\Delta t = t_{i+1} - t_i$ (t-evolve of the Wolf *et al.* algorithm, since $L(t_i) \sim e^{\lambda (t_i - t_0)} L_0(t)$). In contrast, for large values of the evolution time the trajectories on the strange attractor converge and the estimated values of L_{max} are low. This enables us to explain the big difference between variations (ΔL_{max}) in the Lyapunov exponents when the evolution time step changes in both real and colored noise data. Qualitative evidence for a supposed magnetospheric strange attractor is also given by three-dimensional phase portraits of AE and PS ***B*** field data presented in Fig. 6a and b, while Fig. 6c shows the three-dimensional phase portrait of a colored noise with an a of 1.5. These portraits include 3000 reconstructed 3-dimensional vectors. For their construction we used a time delay equal to the decorrelation time for each time series. It is obvious from these pictures that, in the case of colored noise, we observe a random Brownian motion. In contrast, for real data we have a rich structure which possibly corresponds to the three-dimensional projection of a smooth orbit traced in a phase space with $2D + 1$ dimensions.

Although the above results strongly indicate a magnetospheric strange attractor, the possibility of a colored noise theoretically remains open until a reliable model with chaotic dynamics can be obtained for magnetospheric dynamics. However, it is important to stress here that the physical meaning of colored noises with low-di-

mensional chaotic dynamics profiles could be under dispute in some respects. Gershenfeld (1990) showed that a noise with power spectrum $P(f)$ of $1/f^a$ obtained from some standard electrical sources cannot be explained by deterministic models with fewer than 20 degrees of freedom. Of course, this result cannot completely exclude the possibility of a pseudo (low-dimensional) chaotic profile caused by some kind of high-dimensional stochastic noisy process. More details about this problem will be presented later.

Solar wind chaotic dynamics

Temperature and magnetic field chaotic analysis

Here we present some first results of the strange attractor analysis for solar wind data. Fig. 7a shows a typical form of solar wind temperature measurements in situ near the earth. The time resolution is 1 h and the time series length is $N = 12\,000$. The corresponding autocorrelation coefficient presented in Fig. 7b decays abruptly to zero after about 80 h of lag time. In contrast, the colored noise with the same fractal dimension as the temperature time series shows a very slowly decreasing autocorrelation coefficient. Figure 7c describes the power spectrum of the temperature time series. It is clear that it follows a power law $P(f) \propto f^{-a}$ with an exponent a of 1.1 ± 0.1. For a linear fit, we used frequencies lower than about -4.2 Hz. Any other trial of fitting gives $a < 1$.

Figure 8 shows the characteristics for a time series of solar wind magnetic field (SW $\boldsymbol{B}$) data. The SW $\boldsymbol{B}$-field autocorrelation coefficient decreases abruptly to zero after about 40 h, while the corresponding colored noise autocorrelation coefficient decreases very slowly. Clearly, colored noises having similar fractability (correlation dimension) to SW temperature and SW $\boldsymbol{B}$-field data become decorrelated very slowly (the first zero of the correlation coefficient occurs at about 1500 units of lag time) in contrast to real SW time series which become decorrelated after 40–80 h. The power spectrum of the SW $\boldsymbol{B}$-field also follows a power law $P(f) \propto f^{-a}$ with a about 1.8 ± 0.2. Figure 9 summarizes the correlation dimension analysis for the SW data. The fractal dimensions found were 4.5 for the SW $\boldsymbol{B}$ field data and 4.8 for the SW temperature data. Figure 10 shows the estimates of the largest Lyapunov exponents L_{max} for both the SW data and a colored noise time series with fractal dimension 4.5, which is similar to that of the SW time series. As in the case of the magnetospheric time series, the positive LEs for the SW temperature and SW $\boldsymbol{B}$-field time series are obviously dependent upon the evolution time step. In particular, Fig. 10a shows the temperature LE which stabilizes at 0.3 bit/h and 0.1 bit/h, for evolution time steps of 3 and 10 h respectively. For the SW $\boldsymbol{B}$ field time series (Fig. 10b) we observe that the stabilizing values of the LEs are 0.15 and 0.07 for the same evolution time steps. The corresponding values in the case of colored noise time series (Fig. 10c) are one order of magnitude lower. Also the estimated variation in the SW data, ΔL_{max}, which is obtained by changing the evolution time step, is

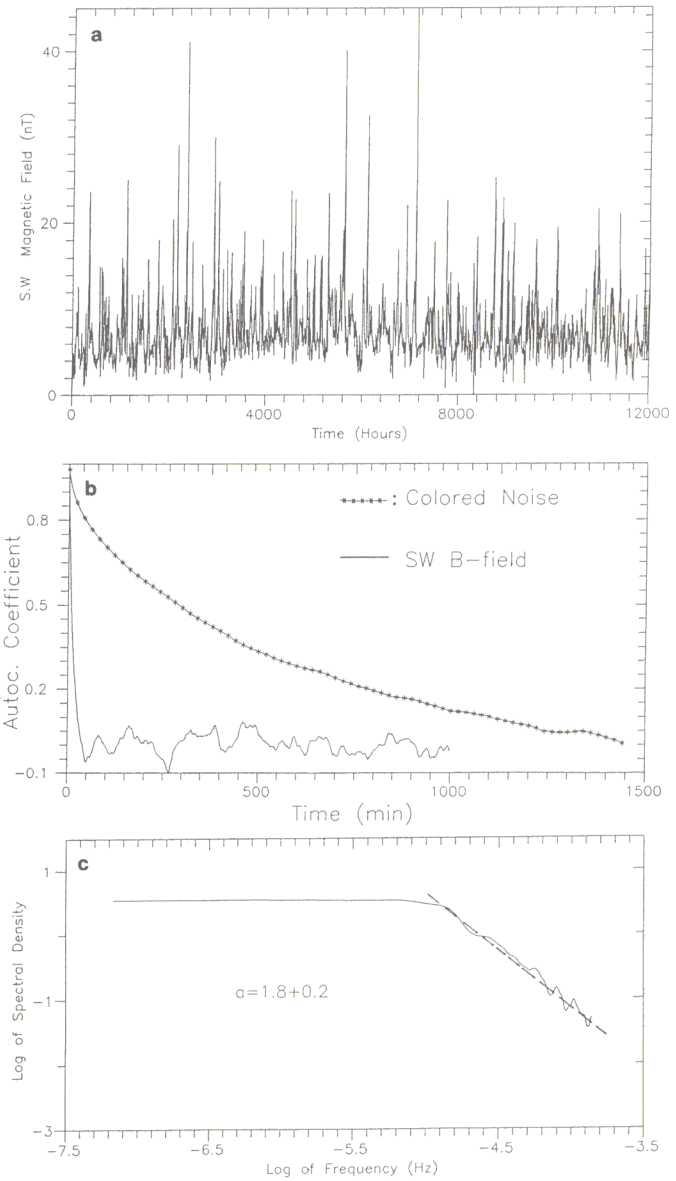

Fig. 7. **a** Solar wind (SW) temperature data with 1-h time resolution measured in situ in interplanetary space, **b** the autocorrelation coefficient for the SW temperature data and a colored noise with the same fractal dimension as the SW temperature data, **c** the power spectrum of the SW temperature data

0.2 bit/h for the SW temperature and 0.08 bit/h for the SW $\boldsymbol{B}$-field. In the case of the colored noise, L_{max} is almost one order of magnitude lower than this. The variations in SW data ΔL_{max} are 5–10 times higher than the variations in colored noises.

Discussion

The above results support the supposition of low-dimensional chaotic dynamics of the solar wind. The coincidence of the correlation dimension by two different kinds of data was remarkable, being 4.5 for the magnetic field time series and 4.8 for the temperature time series. Moreover, if the real time series behaved as colored noises with

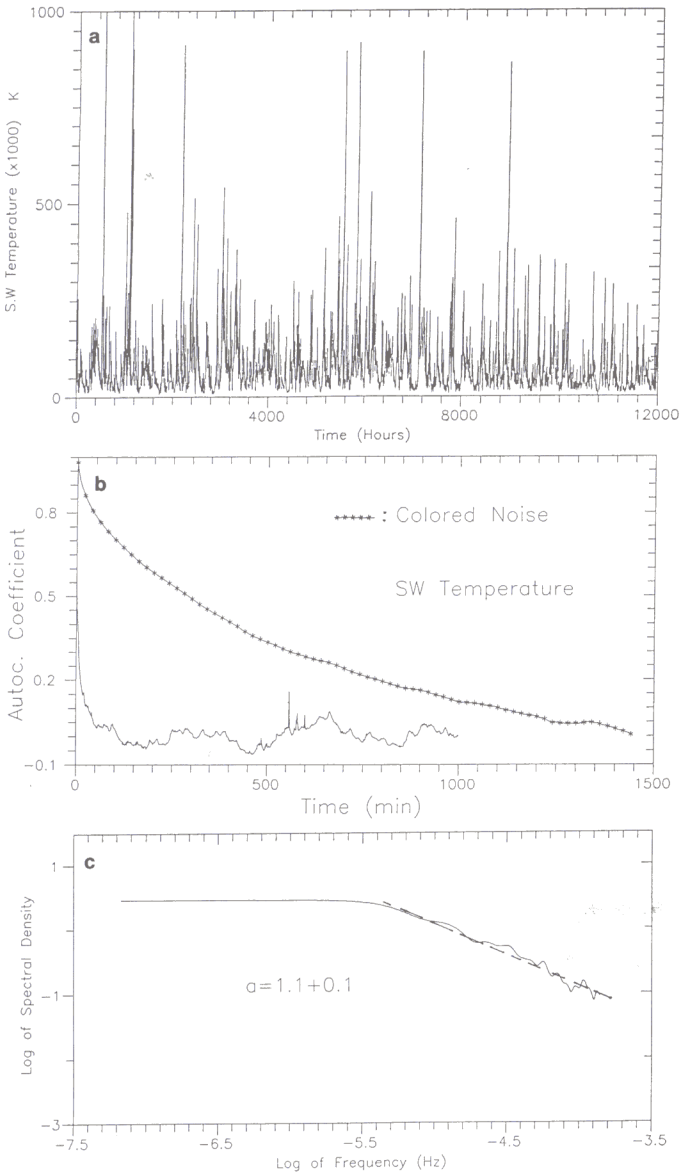

Fig. 8a–c. Same plots as in Fig. 7 for the solar wind magnetic field time series

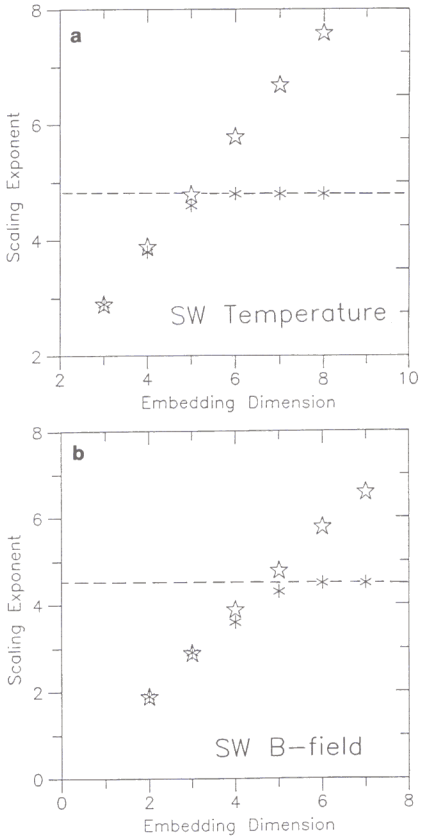

Fig. 9a, b. The scaling exponent as a function of embedding dimension for: **a** the SW temperature time series and **b** the SW ***B***-field time series

identical power spectra, then the estimated dimension D should be higher than 20 for the temperature data and about 1–3 for the magnetic field data. These values are clearly different from the estimated values, 4.5 and 4.8, of the correlation dimensions for SW time series. Also, in the case of colored noise with a D of 4.5, which corresponds to $a = 1.44$, the decorrelation time should be 2000 units, as is shown in Figs. 7b and 8b. This value is about two orders of magnitude larger than the temperature (80 h) and the magnetic field (40 h) decorrelation times estimates for our data. We thus believe that we also have strong evidence about a strange attractor structure for the solar wind dynamics with fractal dimension 4.5–5.0.

Figure 11 shows three-dimensional phase portraits for the SW temperature and SW ***B***-field data (Fig. 11a, b), while Fig. 11c shows the three-dimensional phase portrait for a colored noise time series with fractal dimension 4.5, similar to the fractal correlation dimension of the SW time series. These figures reveal a rich structure for the SW data which possibly corresponds to the three-dimensional projections of smooth trajectories evolved in higher spaces, while the colored noise time series simply shows Brownian motion with an almost homogeneous spatial distribution.

More tests for the exclusion of low-dimensional colored noises

Although the above results gave significant evidence for the presence of a low-dimensional chaotic attractor in space plasma dynamics, the possibility for different interpretations is still open. Some arguments to exclude the possibility of a pseudo-chaotic profile related to random noises studied in Osborne and Provenzale (1989) have already been presented. However, this kind of noise doesn't eliminate entirely the stochastic processes with convergent dimension. For this reason, we discuss in this section more tests about the possibility of pseudo-chaotic behaviour which would be associated with a nonlinear stochastic process. This process would not necessarily be generated by chaotic dynamics. For nonlinear noises, phase randomization destroys the multifractal nature of the process but it does not significantly alter the value of

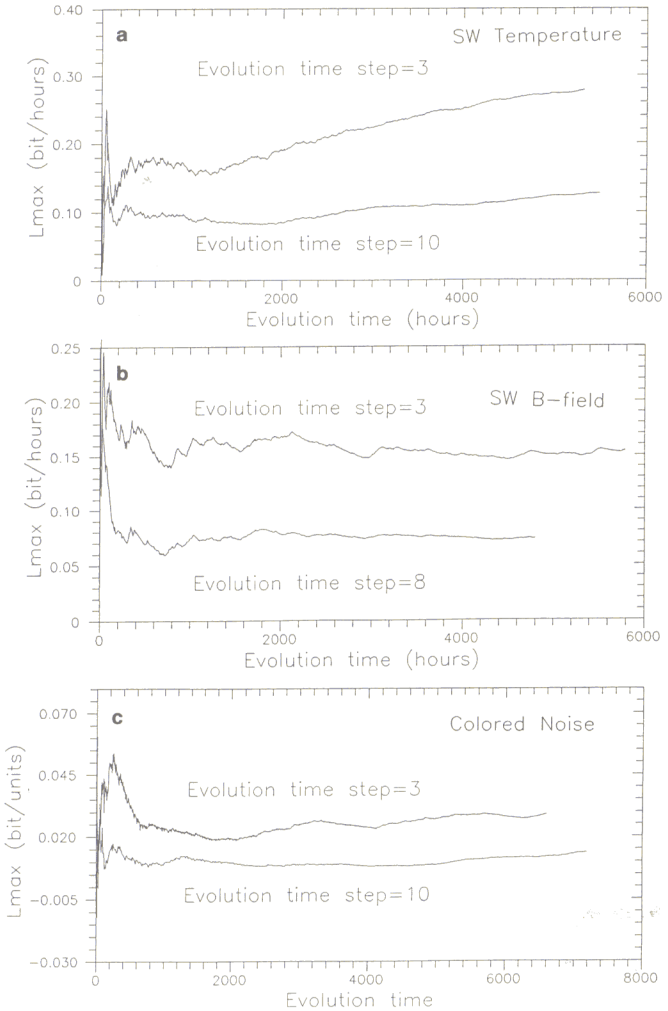

Fig. 10a–c. Some plots as in Fig. 5 for the SW data

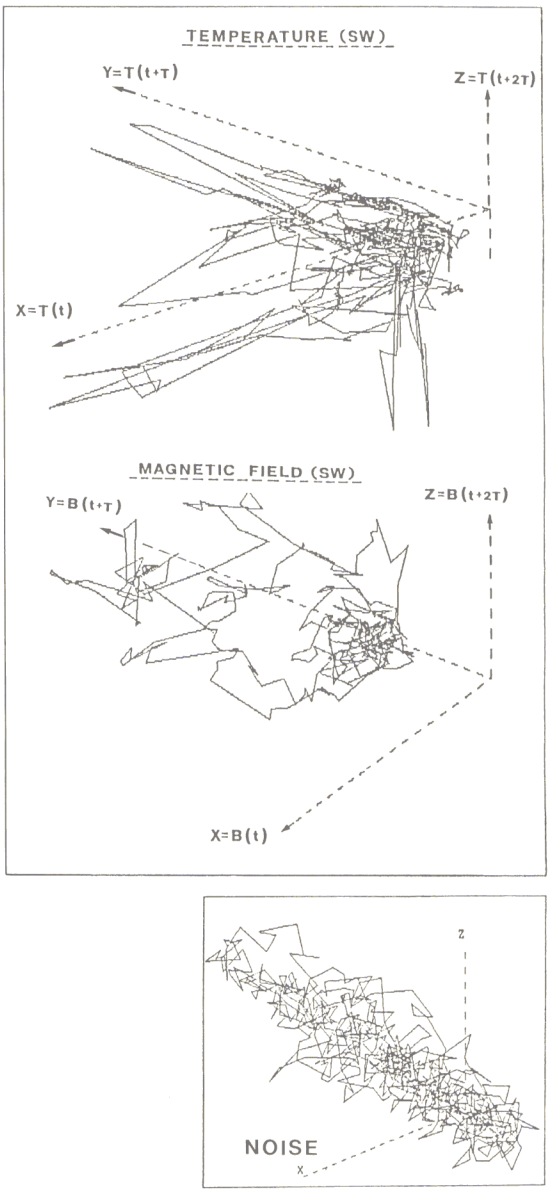

Fig. 11. Three-dimensional portraits for the SW data and the corresponding colored noise

the correlation dimension. Thus we use the Fourier presentation of our time series:

$$x(t_i) = \sum_k C_k \cos(\omega_k t_i + \varphi_k),$$

where φ_k are the phases and C_k are constants.

The randomization of phases transforms the original time series to a colored noise. If the low-dimensional chaotic profile of the original time series is caused by a noisy stochastic process, then this profile must remain invariant after the randomization of the phases. In the case of a deterministic chaotic signal, phase randomization can destroy the low-dimensional chaotic profile. Figure 12a–d shows the slopes of the correlations integrals for the magnetospheric and solar wind randomized time series. It is clear that randomization destroys the chaotic profile of the original time series, since these figures do not reveal any saturation of the scaling exponent (which corresponds to the correlation dimension) to a value lower than 10.

Moreover if we suppose that the power law $P(f) \infty f^{-a}$ of the power spectra described above for the space plasma time series is the result of a colored noise process, then it is interesting to study the stationary or non-stationary character of the time series. Colored noises with pseudo-chaotic (low-dimensional) profiles are self-affine fractional Brownian random signals (Osborne and Provenzale, 1989). A random signal $x(t_i)$ $(i = 1, 2, \ldots, N)$ is said to be self-affine if the relation

$$x(t_i + b\,\Delta t) - x(t_i) \overset{\text{av}}{=} b^H [x(t_i + \Delta t) - x(t_i)]$$

holds independent of time. $\overset{\text{av}}{=}$ means, equality for average values over all the points, while H is known as the scaling exponent. For $0 < H < 1$, m independent random self-affine signals $x_n(t_i)$ $(n = 1, 2, \ldots, m,\ i = 1, 2, \ldots, N)$ can form a self-similar fractal curve in a m-dimensional space. According to Mandelbrot (1982), in such a self-similar random path the fractal dimension D_H is given by the relation

$$D_H = \min\{1/H, m\}.$$

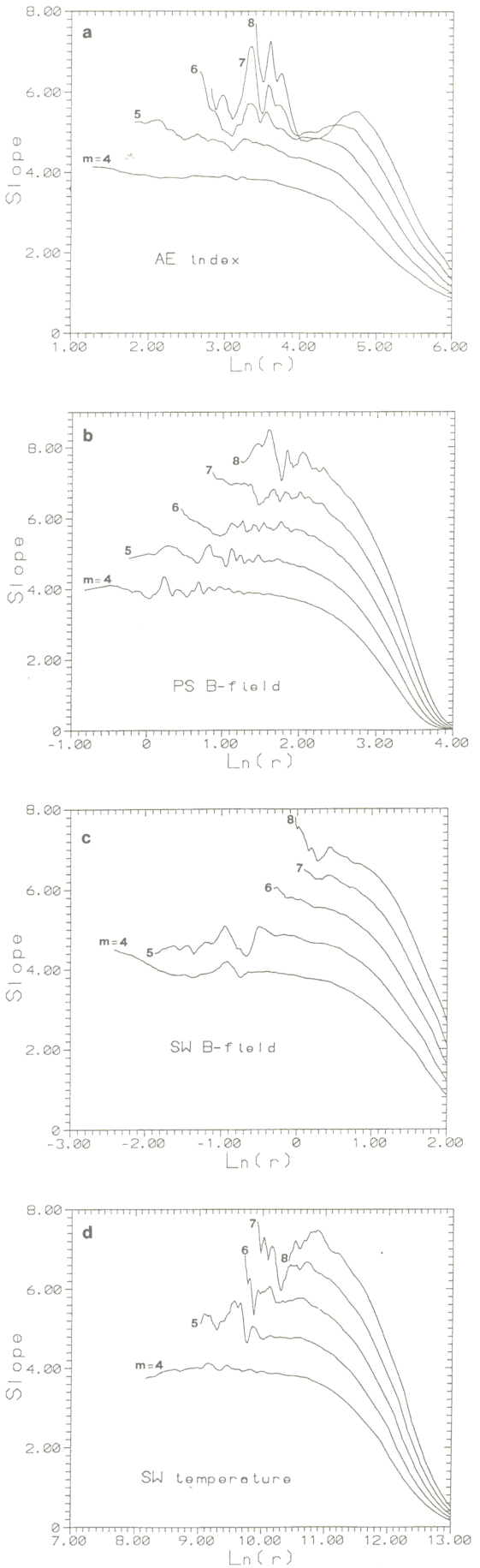

On the other hand it is known that a self-affine signal has a power-law spectrum $P(f) \propto f^{-a}$ with $a = 2H + 1$. It is clear now that, for $1 < a < 3$, the Grassberger and Procaccia approach (1981) cannot distinguish between fractal attractors and fractal random curves of the same dimension.

For a fractional self-affine random signal, it can be proved that the average increments $[x(t_i) - x(t_0)]_{av}$ are zero while the variance of the increments $V(t_i - t_0)$ given by the average of $[x(t_i) - x(t_0)]^2$ diverges with time according to the relation

$$V(t_i - t_0) \sim (t_i - t_0)^{2H}$$

(Feder, 1988). This means that fractional Brownian motions with colored noise profiles, although they can have low fractal dimension, are not stationary signals, unlike motions on strange attractor structures.

So if we are able to assert the stationarity of space plasma time series, then the fractional Brownian motion could be excluded. In order to test the stationary of a random physical process we can use a measure $\varrho(\boldsymbol{x})$ of the probability density in phase space. For a stationary process, $\varrho(\boldsymbol{x})$ must be invariant with time; while the same must be true for the density projection $\varrho(x_i)$ corresponding to the probability density of the x_i coordinate, for which we have

$$\varrho(x_i)\,dx_i = \int \varrho(\boldsymbol{x})\,dx_1 \ldots dx_{i-1}\,dx_{i+1} \ldots dx_m.$$

We can calculate $\varrho(x_i)$ for one coordinate x_i corresponding to the experimental time series data by dividing the x_i-axis into short intervals and counting the measured points which fall into these intervals. Figure 13 a – d contains the results of the normalized measures $\varrho(x_i)$ for the space plasma time series. The solid line shows the measure $\varrho(x)$ based on the entire time series, while the curve with stars corresponds to the measure $\varrho(x)$ based on the first half of the same time series. The coincidence is very good and the chi-square test for checking the accuracy of fit gives values over 90%. Figure 14 a and b shows $\varrho(x)$ for colored noises with the same fractal dimensions. It is evident that the probability density function $\varrho(x)$ depends strongly upon the length of the time series. The chi-square test shows that the coincidence is very low with values of the test-statistic below 20%. This reveals the nonstationary character of the noise signal in contrast to space plasma time series.

Until now, we have presented four independent tests in order to exclude the possibility of low-dimensional pseudo-chaotic dynamics in space plasmas. These were: a) the comparison of the correlation dimension (D) with the power spectra profile (a) according to the relation $D = 2/(a - 1)$; b) The comparison of the autocorrelation function profiles of the space plasma time series and the colored noises with the same fractal dimension; c) phase

Fig. 12 a–d. Slopes $d \ln C(r;m)/d \ln(r)$ corresponding to time series with randomized phases for: **a** AE index, **b** plasma sheet B-field, **c** solar wind temperature, **d** solar wind B-field. These plots were calculated for embedding dimensions $m = 4, 5, 6, 7, 8$

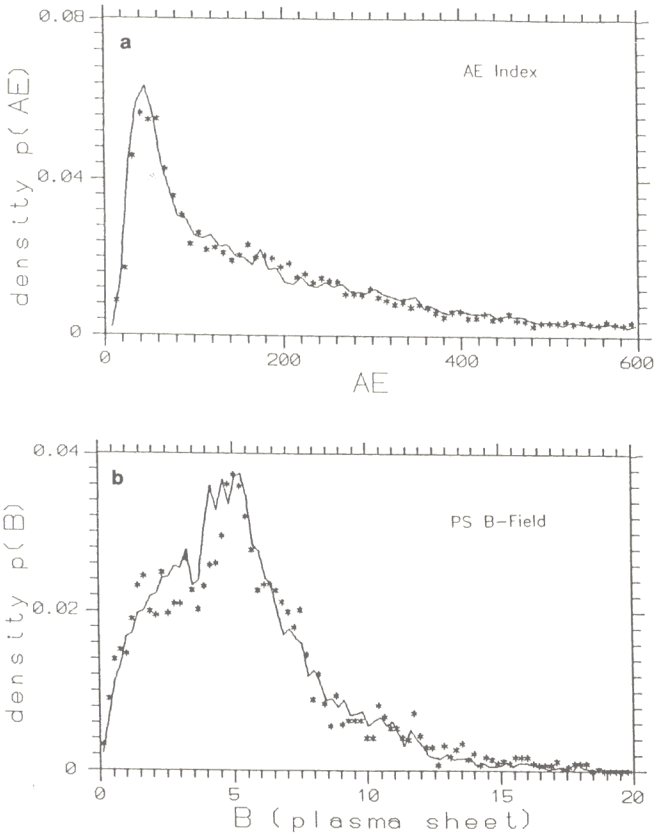

Fig. 13a–d. Probability density functions $\varrho(x)$ based on the entire time series (solid line) and on the first half of the time series (stars) for: **a** AE index, **b** plasma sheet B-field, **c** SW temperature and **d** SW B-field

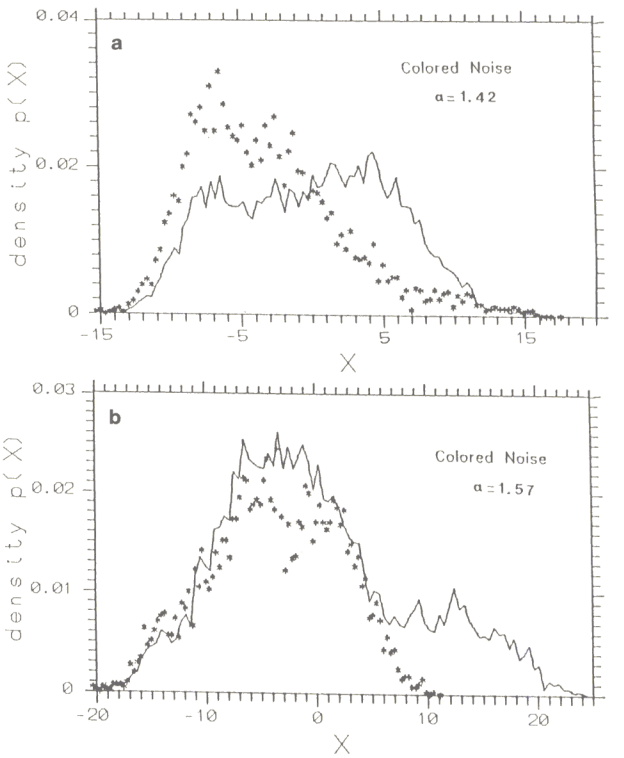

Fig. 14a, b. Similar plots to those of Fig. 13 for colored noises with correlation dimensions 4.5 and 3.5

randomization of the initial time series, which produced random signals showing that there is no saturation of the scaling exponents at values lower than 10; and d) the stationarity of the space plasma time series in contrast to the nonstationary character of fractal Brownian signals. These tests support the view that the low values of the fractal dimensions and the positive Lyapunov exponents found here for space plasma time series may be caused by strange attractor dynamics. However, the problem of noise is still open, as it is reasonable to accept the presence of a noisy component in our time series. So, in the following we apply the Grassberger-Procaccia algorithm to time series which are derived from the initial time series after moving average (or running average) smoothing or differencing. A possible theoretical framework within which we can handle practical problems is a model of the form

$$X(t_i) = \mu(t_i) + U(t_i)$$

where $X(t_i)$ is the initial time series, $\mu(t_i)$ is the trend of the $X(t_i)$ and $U(t_i)$ is a stationary stochastic series. By applying a moving average smoothing technique, we reduce the stochastic component $U(t_i)$, while differencing removes the trend of our time series. The relation

$$S(t_i) = [X(t_{i-1}) + X(t_i) + X(t_{i+1})]/3$$

was used for the smoothing of our time series, while the relation

$$\nabla X(t_i) = X(t_i) - X(t_{i-1})$$

was used for the differencing.

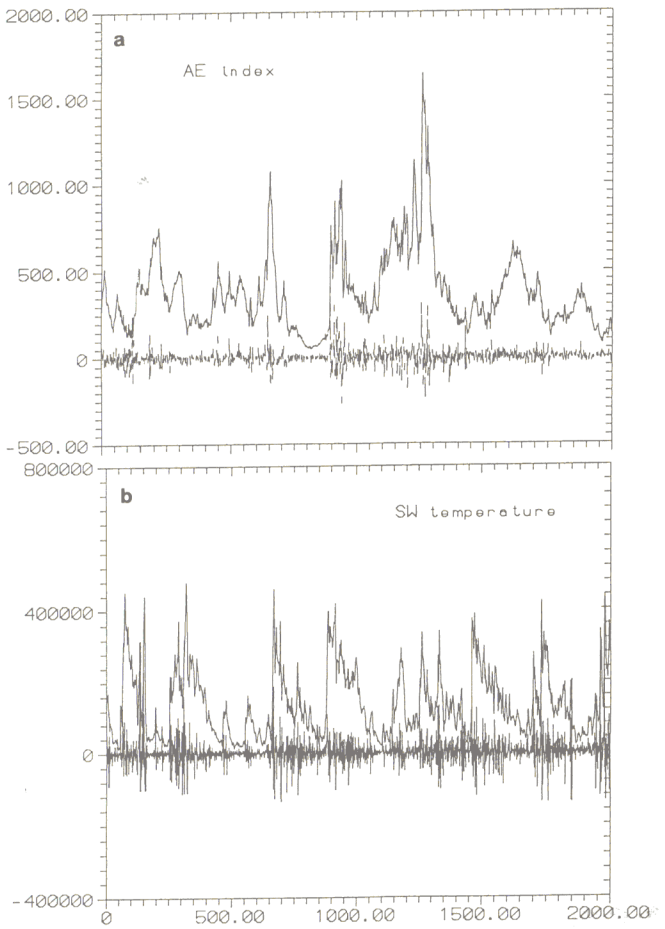

Fig. 15. **a** A short part of the smoothed AE index time series (solid line) and of the first differences (broken line), **b** same plots as (a) for the SW temperature time series

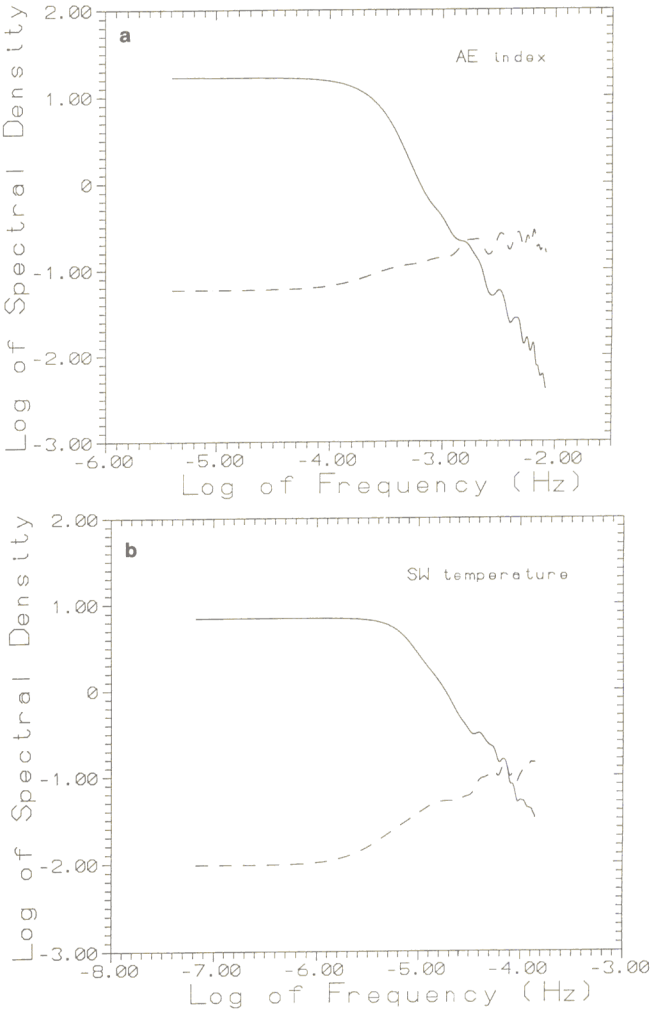

Fig. 16. **a** Power spectrum for the smoothed AE index (solid line), **b** power spectrum for the first differences of the AE index

Figure 15a shows the first 2×10^3 points of the smoothed AE index (solid line) and the first 2×10^3 points of the first differences (broken line). Figure 15b shows the same curves for the solar wind temperature (TSW) time series. Figure 16a and b shows the corresponding power spectra for the smoothed time series (solid line) and the first differences (broken line). It is important to note that the power spectra of the smoothed time series is similar to the spectra of the original time series (Figs. 1c and 8c). However, differencing gives a power spectrum similar to white noise, since it acts as a high pass filter, which permits the high frequencies to pass but significantly weakens the low frequencies. It is apparent that differencing acts as an amplifier of the noisy component included in the original time series. This is in accordance with the results of the Grassberger-Procaccia algorithm applied to the smoothed time series (Fig. 17a and b) for the first differences (Fig. 18a and b). Figure 17a and b shows the slopes of the correlation integrals for the smoothed AE index and TSW time series for embedding dimensions $m = 4, 5, 6, 7, 8$, while Fig. 18a and b shows the same slopes for the first differences of the AE index and TSW time series. It is interesting to note that, in the case of smoothing, there is a clear saturation of the scaling exponent at 2.8 for the smoothed AE index and 4.3 for the smoothed TSW time series. These values are clearly lower than the saturation values 3.5 and 4.8, which were estimated for the original AE and TSW time series. In contrast, differencing does not reveal any saturation, at least for embedding dimensions, m, lower than 10 in both cases. This characteristic can be explained if we suppose that differencing cuts the low-dimensional chaotic component of the original time series and leaves the purely stochastic (high-dimensional) noisy components of the time series unaltered. Similar results were obtained for the time series of the plasma sheet and solar wind magnetic field.

Summary and discussion

In this work we applied a strange attractor analysis to magnetospheric and solar wind data. This analysis gave us strong evidence for the existence of low-dimensional chaotic dynamics in space plasmas, especially in magnetospheric and solar wind systems. Although the road for different interpretations (stochastic pseudo chaotic profile) is not entirely closed, we believe that the calculation of fractal correlation dimensions (2.5–3.5 for the magne-

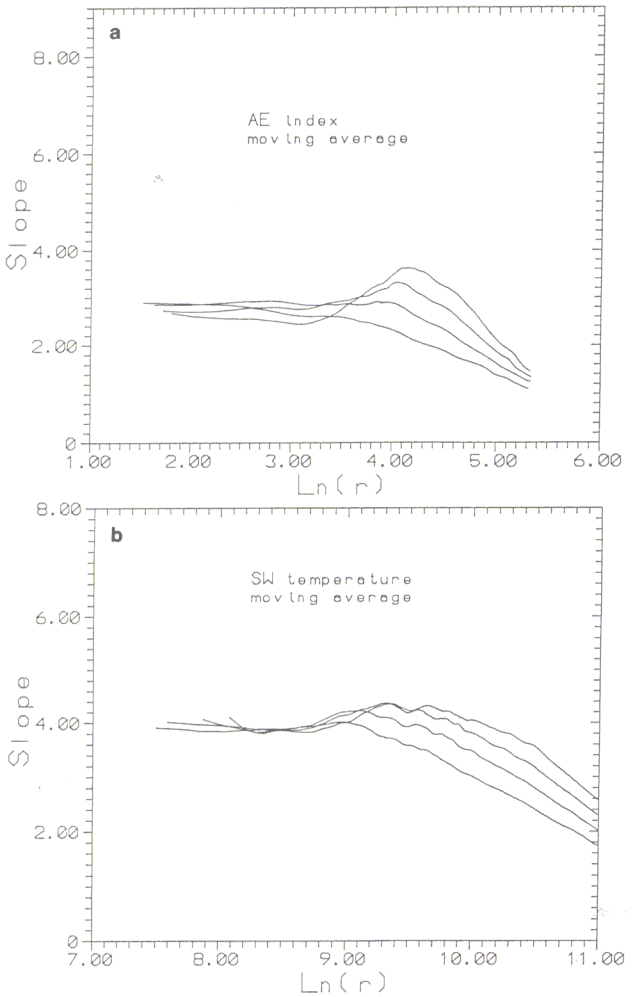

Fig. 17. **a** Slopes $d \ln C(r; m)/d \ln (r)$ corresponding to the smoothed AE index time series for embedding dimensions $m = 4, 5, 6, 7$, **a**, **b** same plots as (a) for the SW temperature time series

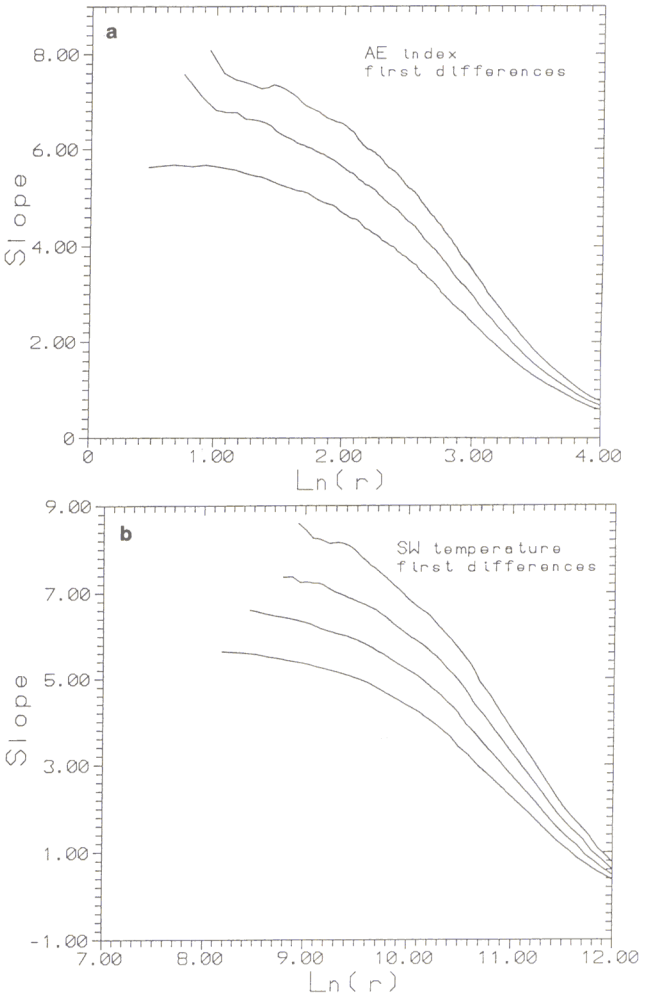

Fig. 18. **a** Slopes $d \ln C(r; m)/d \ln (r)$ corresponding to the first differences of the AE-index for embedding dimensions $m = 4, 5, 6, 7, 8$, **b** same plots as (a) for the SW temperature time series

tospheric plasma system and 4–5 for the solar wind plasma), the positive Lyapunov exponents and the three-dimensional phase portraits for the magnetospheric and solar wind time series support the supposition of deterministic chaos. However, this supposition must be tested more carefully with prediction algorithms which could help to distinguish more efficently between purely stochastic (noisy) and chaotic (deterministic) processes. Some interesting results in this direction in space plasma dynamics will appear in the near future.

At this point we must note that the supposition of deterministic chaos is not without physical meaning for space plasmas, as these are nonlinear and dissipative systems. It is becoming apparent that the theory of strange attractors finds many applications in a wide variety of physical situations, such as the onset of turbulence in fluid, nonlinear wave interactions in plasmas, self-generation of the earth's magnetic field magnetohydrodynamic flow, etc. (Ott, 1981). For nonlinear and dissipative (open) systems, some kind of non-local self-organizing process is present. This implies the reduction in the infinite number of degrees of freedom (as happens with plasma) to a few macroscopic degrees of freedom which are sufficient for the description of the global dynamics of the system. A mathematical description of this process could be obtained by using the slaving principle (Haken 1983). According to this principle, a dissipative system, possibly with infinite modes $S_k = \varrho_k + i e_k$, permits some kind of distinction between a finite number of unstable slow modes ($\varrho_k > 0, k = 1, 2, \ldots, n$) and an infinite number of stable fast modes ($\varrho_k < 0$). Then the finite slow (unstable) modes slave the stable fast modes and reduce the macroscopic dynamics of the system to a low dimensional subspace of the original infinite dimensional phase space. The finite unstable modes ($\varrho_k > 0$, $k = 1, 2, \ldots, n$) are characterized as order parameters and define the low-dimensional phase space of the system, while the evolution of the system state in phase space can be asymptotically reduced to a fractal set which has the characteristics of a strange attractor. These characteristics are a low fractal dimension and a sensitivity to the initial conditions of the system dynamics. The existence of at least one positive Lyapunov exponent is the consequence of these characteristics. Moreover, when the dynamics of the system evolves on a strange attractor (attracting set), then Poincaré sections on two or three dimensional hyperplanes it is possi-

ble to reveal simple ordered structures. For the magnetospheric plasma we could assume as order parameters the elements of the magnetospheric equivalent electric circuit which constitute a nonlinear chaotic system. Such a nonlinear model for magnetospheric dynamics has already been developed by a suitable physical extension of the linear magnetospheric equivalent electric circuit. It is significant to note that the time series obtained by solving this nonlinear magnetospheric model numerically showed similar chaotic characteristics to those described above for the AF index and the plasma sheet magnetic field time series. These results are under preparation and will appear in the near future.

In relation to a solar wind magnetized plasma system, the order parameters which describe the low-dimensional chaotic dynamics (if we believe that this is a correct interpretation of the results presented here) must be derived by an appropriate generalization of the Lorenz model. For a magnetized conductive fluid (as happens with space plasmas in the MHD approximation) the system of partial differential equations which describes the fluid must also include the Maxwell equations. This means that the Lorenz approximation must be extended to the entire MHD system of equations. This is in physical agreement with the fractal dimension 4.5 which has been estimated above for the solar wind dynamcis.

Finally we believe that the complete verification of the existence of strange attractors in space plasmas dynamics will be better explained by: (a) the construction of appropriate nonlinear models, as described above; and (b) the development of prediction codes. We already have some encouraging results for the prediction of the experimental time series presented in this work.

Acknowledgements. The authors wish to thank Prof. A. R. Osborne for his helpful remarks. Also we thank R. P. Lepping (Goddard Space Flight Center) for the IMP magnetometer data, and T. Araki and T. Kamei (World Data Center C2 for Geomagnetism, Kyoto University) for the supply of one-minute AE index tapes. We are most grateful to the two referees for their constructive comments, which led to the presentation of this paper.

References

Baker, D. N., A. J. Klimas, R. L. McPherron, and J. Buchner, The evolution from weak to strong geomagnetic activity: an interpretation in terms of deterministic chaos. *Geophys. Res. Lett.*, **17,** 41–44, 1990.

Brillinger, D. R., Time series: Data analysis and theory, Holt, Rinehart and Winston, New York, 1981

Burlaga, L. F., Multifractional structure of the interplanetary magnetic field, *Geophys. Res. Lett.*, **18,** 69–72, 1991.

Eckmann, J. P., Roads to turbulence in dissipative dynamical systems. *Rev. Mod. Phys.*, **53,** 643–654, 1981.

Eckmann, J. P., and D. Ruelle, Ergodic theory of chaos and strange attractors, *Rev. Mod. Phys.*, **57,** 617–656, 1985.

Farmer, J. D., Spectral broadening of period-doubling bifurcation sequences, *Phys. Rev. Lett.*, **47,** 179–182, 1981.

Feder, J., Fractals, Plenum Press, New York, 1988.

Gershenfeld, W., Measuring large dynamical dimension. Dimension measurement in high-dimensional systems, *Ph.D. Thesis, School of Applied and Engineering Physics, Cornell University,* Ithaca, N.Y., 1990.

Grassberger, P., and I. Procaccia, Characterization of strange attractors, *Phys. Rev. Lett.*, **50,** 346–349, 1981.

Haken, H., Advanced synergetics, Springer, Berlin Heidelberg New York, 1983.

Hundhausen, A. J., Coronal expansion and solar wind, Springer, Berlin Heidelberg New York, 1972.

Mandelbrot, B., The fractal geometry of nature, Freeman, San Francisco, 1982.

McPherron, R. L., Magnetospheric substorms, *Rev. Geophys. Space Phys.*, **17,** 657–681, 1979.

Nerenberg, M. A. H. and C. Essex, Correlation dimension and systematic geometric effect, *Phys. Rev. A,* **42,** 7065–7064, 1990.

Osborne, A. R., and A. Provenzale, Finite correlation dimension for stochastic systems with power-law spectra, *Physica D,* **35,** 357–381, 1989.

Ott, E., Strange attractors and chaotic motions of dynamical systems, *Rev. Mod. Phys.*, **53,** 655–671, 1981.

Parker, T. S., and L. O. Chua, Chaos: a tutorial for engineers, in *Proceedings of the IEEE,* **75,** 982–1008, 1987.

Pavlos, G. P., Magnetospheric dynamics, in *Proceedings of the Symposium on Solar and Space Physics,* 1–43, National Observatory of Athens, Greece, 1988.

Pavlos, G. P., and E. T. Sarris, Encounter with a source of energetic particles inside the plasma sheet, *Ann. Geophysicae,* **7,** 531–540, 1989.

Pavlos, G. P., E. T. Sarris, and N. Paschalidis, The growth rate and location of the acceleration of energetic particles inside the plasma sheet, *Planet. Space Sci.*, **37,** 503–516, 1989.

Rostoker, G., The Kelvin-Helmholtz instability and its role in the generation of the electric currents associated with Ps 6 and westward travelling surges, in *Magnetotail Physics,* Ed. A. T. Y. Lui, 169–173, Johns Hopkins University Press, Laurel, Md, USA, 1987.

Schuster, H. G., Deterministic chaos, VCH Verlagsgesellschaft, Weinheim, 1989.

Shan, L. H., P. Hansen, C. K. Goertz, and K. A. Smith, Chaotic appearance of the AE index, *Geophys. Res. Lett.*, **18,** 147–150, 1991.

Smith, L. A., Intrinsic limits on dimensional calculations, *Phys. Lett. A,* **133,** 283–288, 1988.

Takens, F., Detecting strange attractors in turbulence, in *Lecture Notes in Mathematics,* Eds. D. A. Rand and L. S. Young, Vol. 898, 366–381, Springer, Berlin Heidelberg New York, 1981.

Vassiliadis D. V., A. S. Sharma, T. E. Eastman, and K. Papadopoulos, Low-dimensional chaos in magnetospheric activity from AE time series, *Geophys. Res. Lett.*, **17,** 841–844, 1990.

Wolf, A., J. B. Swift, H. L. Swinney, and J. Vastano, Determining Lyapunov exponents from a time series, *Physica D,* **16,** 285–317, 1985.